IP2016 / 4th International Workshop on Induced Polarization

Decay-Curve Analysis for the Quantification of Data Error in Time-Domain Induced Polarization Imaging

Adrián Flores Orozco
TU-Wien
Vienna, Austria
Flores@tuwien.ac.at

Jakob Gallistl
TU-Wien
Vienna, Austria
Jakob.Gallistl@geo.tuwien.ac.at

Matthias Bücker
TU-Wien
Vienna, Austria
Matthias.Buecker@geo.tuwien.ac.at

Kenneth H. Williams
Lawrence Berkeley National Lab
Berkeley, California, USA
khwilliams@lbl.gov

SUMMARY

Recent studies have demonstrated the advantages of a careful processing of induced polarization (IP) imaging datasets. In particular, inversion results based on an adequate quantification of data error provide IP images with enhanced contrasts and a better correlation with subsurface structures and processes. The analysis of the discrepancy between normal and reciprocal readings is a widely accepted measure to assess quality of imaging datasets and parametrize error models. However, the collection of reciprocal measurements increases acquisition time and is not always feasible. Therefore, we propose an alternative methodology to quantify data error of time-domain IP (TDIP) imaging measurements based on the analysis of the recorded IP decay curve. Our approach provides detailed information about data error as required for the identification of outliers and the quantification of error parameters without the need of reciprocal measurements. Comparison of the error parameters and imaging results following our proposed decay-curve analysis (DCA) and the conventional normal-reciprocal analysis revealed consistent results, demonstrating the accuracy of our approach. We illustrate the practical applicability of our approach with the inversion results for an extensive field data set collected at the floodplain scale aiming at the localization of so-called "biogeochemical hot-spots", which are areas characterized by high rates of microbial activity and the accumulation of iron sulphides.

Key words: data processing, error quantification, time-domain IP, hydrogeophysics, biogeophysics.

INTRODUCTION

Initially developed for the prospection of metallic ores, the induced polarization (IP) method has emerged in recent years as a suitable technique for hydrogeological studies. As an extension of the standard DC-resistivity method, IP measurements provide information about the electrical conductivity (i.e., energy loss) and polarization (i.e., energy storage) properties of the subsurface, permitting an improved lithological characterization. Furthermore, studies using multi-frequency measurements (spectral-IP, SIP) have demonstrated the ability of the IP method to gain information about biogeochemical processes. For instances, an increase in the polarization effect has been correlated to the accumulation of bio-films in column experiments (e.g., Ntarlagiannis et al., 2005). Also, a significant increase in the polarization response has been observed due to the precipitation of metallic minerals accompanying the stimulation of microbial activity (e.g., Williams et al., 2009; Flores Orozco et al., 2011). Furthermore, changes in the electrical signatures have been correlated to reversible chemical transformation of bio-minerals (e.g., Slater et al., 2007; Flores Orozco et al., 2013). Such results have promoted the application of the IP method in numerous investigations in the emerging discipline of biogephysics (e.g., Atekwana and Slater, 2009). Built on these findings, a recent study has explored the applicability of the IP imaging method for the prospection of naturally reduced zones (NRZ) at the floodplain scale with promising results (Wainwright et al., 2016). NRZ are spatially limited areas characterized by high rates of microbial activity and thus a disproportionally large impact on larger-scale biogeochemical cycling. Furthermore, chemical changes in the groundwater composition accompanying microbial activity in NRZ might be associated with the precipitation of metallic minerals, such as iron sulphides (FeS), which have a measurable polarization effect.

Site characterization at the floodplain scale based on the analysis of soil and groundwater samples is limited by the characteristics of the samples (e.g., location of the boreholes, depth and volumes of the sampling), and often lacks the spatial resolution needed to identify NRZ. IP images provide information about the electrical properties of the floodplain sediments at a high spatial resolution and might be a suitable alternative to define NRZ. However, as pointed out by Wainwright et al. (2016), the modest polarization response of metallic biominerals places high demands on the resolution of the TDIP imaging results.

An adequate characterization of data error is critical to avoid the creation of artifacts or the loss of resolution in images. Furthermore, quantitative information on data error can be used i) to remove outliers associated with systematic error and ii) for the parameterization of error models describing the characteristics of inherent random error. Flores Orozco et al. (2012) recently adopted a power-law error model to characterize the data error in IP measurements (i.e. phase or chargeability) yielding an improved resolution of the images obtained from an inversion scheme, where the data are fitted to the confidence interval defined by the error model.

Furthermore, the on-site evaluation of data quality is critical to eventually improve the survey design or increase the signal-to-noise ratio (S/N). However, to date, the most widely accepted approach to evaluate IP data quality is based on the analysis of the misfit between normal and reciprocal measurements, where reciprocal measurements are those collected with interchanged current and potential electrodes. Though, the necessity to reduce the acquisition time for large-scale surveys compromises the collection of reciprocals.

Furthermore, measuring configurations characterized by high S/N, such as the multiple-gradient array (Dahlin and Zhou, 2006), are not suited for the collection of reciprocals with multi-channel instruments without drastically increasing the acquisition time. Accordingly, IP surveys at the large scale call for the development of new techniques to quickly and though reliably quantify data quality without the need of reciprocal readings.

Here, we propose a new methodology to quantify data-error parameters based on the analysis of the voltage decay of time-domain IP (TDIP) measurements. Inversion of TDIP measurements were performed using error parameters obtained after the analysis of normal-reciprocal misfit (NRM) and with the proposed decay curve analysis (DCA) to evaluate the performance of the proposed algorithm. We demonstrate the applicability of the new approach with an extensive TDIP data set collected at the floodplain scale that includes dipole-dipole and multiple-gradient data. The objective of the IP survey was the identification of possible NRZ.

STUDY AREA AND SETTINGS

Figure 1. Layout of the TDIP profiles (red lines) collected at the Shiprock site.

Measurements were collected at the Shiprock Site (New Mexico, USA) on the grounds of a former uranium-processing facility. The site has been remediated but remanent concentrations of uranium are still observed in water samples. The site's stratigraphy is characterized by three main units: an impermeable clay-rich layer extending from the surface to ~2 m depth, followed by a sandy-gravel aquifer (~3 m thickness) on top of the low permeable Macos Shale. Groundwater level was located at a depth ~3m during the field surveys. Studies on similar sites (Wainwright et al., 2016) revealed that fluvially deposited organic material within aquifer sediments naturally stimulates the activity of subsurface microorganisms leading to both the natural immobilization of uranium and the accumulation of reduced end products (minerals and pore fluids). In order to map these possible hot spots, which are expected to generate measureable IP anomalies, a total of 22 IP profiles were collected. Six long profiles (up to 350 m) helped to fairly characterize large-scale changes in the electrical properties along the floodplain, and 16 shorter profiles were used to improve the resolution of particular areas of interest (Figure 1). TDIP measurements were collected using the Syscal Iris Pro 72 Switch equipment with a square-wave current injection, 50% duty cycle, and a pulse length of two seconds. The voltage decay was measured along 20 windows between 240 and 1840 milliseconds (ms) after current shut-off. All measurements were collected using a separation of 2 m between electrodes and two configurations: 1) Dipole-Dipole (DD) skip-2 and skip-3 (i.e., a length of 6 and 8 m for both current and potential dipoles), and 2) multiple-gradient (MG) configurations (after Dahlin and Zhou, 2006) with 10 potential dipoles (ski-0, skip-1 and skip-2) nested within the current dipole. DD measurements were collected as normal-reciprocal pairs. In order to reduce acquisition time, the depth of investigation was limited to 7 m, which allowed defining the bottom of the aquifer at the upper limit of the Mancos Shale.

The data error in DD measurements was quantified using the bin analysis for the normal-reciprocal misfit and error-models described in Flores Orozco et al. (2012). All data was inverted with CRTomo an algorithm by Kemna (2000), which permits the inversion of the data only to the confidence level determined by the error model. For inversions with CRTomo, chargeability values were linearly converted to frequency-domain phase values (at the fundamental frequency of 0.125 Hz) assuming a constant-phase response (Kemna, 1997).

DECAY-CURVE ANALYSIS

Initial inversion of MG measurements using error parameters of co-located DD datasets resulted in images that were affected by artifacts (not shown here) due to the over estimation of data error. As expected, a more detailed analysis of the decay curves (see Figure 2) revealed smooth curves for measurements associated with high S/N (i.e., low geometrical factors) and increasingly distorted curves for measurements collected with larger separations between the potential and current electrodes (lower S/N, higher geometrical factors). Previous studies reported similar observations and proposed to manually remove measurements associated with an erratic (or increasing) behaviour of the decay curves (e.g., Gazoty et al., 2013; Doetch et al., 2015).

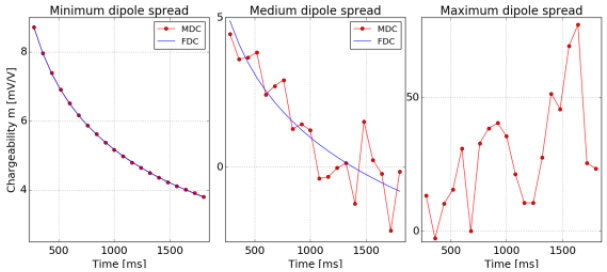

Figure 2. Measured decay curves with DD configurations (red symbols) for small (left), medium (centre) and maximum (right) separation between current and potential dipoles (i.e., S/N). The negative power law model fitted to each curve is indicated with the blue line.

The first step of our processing consists in fitting a negative power-law model (fitted decay curve, FDC) to each measured decay curve (MDC). Such model yields a good fit of most decays while involving a minimum number of parameters. All physically meaningful MDC should be positive and decrease with time. Hence, a first filter removes all measurements associated with non-decaying curves, while measurements associated with an erratic behaviour were not removed. At this point, the actual goodness of the fit is not used for filtering, as this would remove erratic decay curves, typically related to larger separations between electrodes, i.e., "deeper" information, which is critical to solve for accurate images at depth. To explore the robustness of the FDC, we performed a series of analysis. For instances, we compared power-law fits to smaller subsets of the decay curve (odd and even IP windows) or using other models than the proposed power-law fit. Nevertheless, all results were consistent to those using the negative power-law model. To further evaluate the accuracy of the FDC we compared the integral chargeability obtained from the MDC and the FDC, which we found to be very consistent (Figure 3).

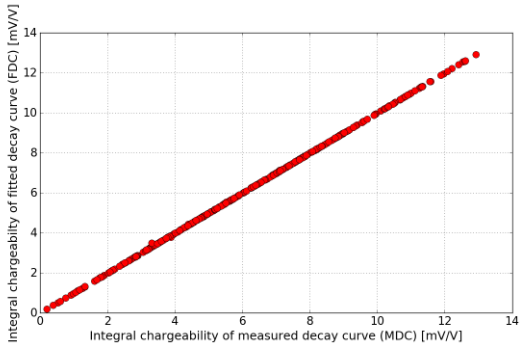

Figure 3. Comparison of the integral chargeability values computed from measured (MDC) and fitted (FDC) decay curves.

To this point each FDC has been fitted independently, which might still result in a high spatial variability of the fitted models. However, due to the nature of the tomographic measurements, chargeabilities are expected to vary in a relatively smooth manner. Therefore, the second step of our analysis assesses the spatial consistency of all FDC of a tomographic dataset to identify and remove outliers. To this end, we compute a master decay curve as the median value of all measurements, and then adjust its position along the y-axis (i.e., the magnitude of the voltage values) to each individual MDC. The resulting curve, i.e. the shifted master decay curve, defines an improved FDC for each measurement. Outliers are then defined as those measurements associated with a large discrepancy between the MDC and the master decay curve.

The filtered DD pseudosections in Figure 4 show that both NRA- and DCA-based filters consistently remove most outliers. Yet, the DCA filter removes fewer measurements associated with relatively high integral chargeabilities and/or small separations between electrodes. This illustrates the main difference between the two approaches. While the DCA only evaluates the similarity of all MDC in a data set with the shape of the master decay curve, the NRA is sensible to variations of the offset of the decay curves, the magnitude of which is higher at small dipole spacings and large chargeabilities.

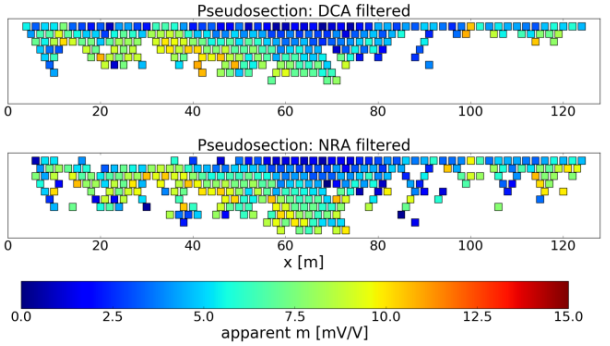

Figure 4. Pseudosection for DD measurements after the removal of outliers as defined by the proposed DCA (top) and standard NRA (bottom).

In a third step, we compute the discrepancy between the MDC and the FDC (fitted in step one), based on the individual misfits for each IP window. This approach allows us to quantify the temporal instability (i.e. erratic behaviour) of the measured signal and use this information to quantify the data error (i.e. standard deviation of a measurement). If we used the misfit of the integral chargeabilities instead, the obtained error would not properly assess the quality of the decay curve. Furthermore, later IP windows are associated with lower voltage values (i.e., lower S/N), thus the analysis of the misfit for each independent window permits a detailed analysis for a larger dynamic in the signal strength. The misfit between FDC and MDC can be used in a similar way as the misfit between normal and reciprocal readings to describe the error of the integral chargeability of a dataset. Figure 5 shows the FDC-MDC misfits and the normal-reciprocal misfit of the same DD data set, both in function of the respective transfer resistances. The patterns of the misfits of DCA and NRA are consistent and exhibit similar power-law distributions.

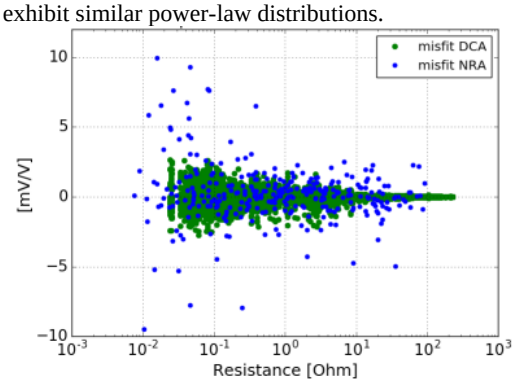

Figure 5. Chargeability error estimates based on DCA- and NRA-misfits plotted as a function of the transfer resistances.

Subsequently, error parameters were obtained for datasets processed by NRA and DCA following the methodology described in Flores Orozco et al. (2012b). Figure 6 presents a comparison of the imaging results for the polarization effect expressed in terms of the phase shift of the complex electrical resistivity. Images of the magnitude of the complex electrical resistivity revealed no significant changes between the two approaches (not shown here). Both phase images consistently resolved the main geological units; the low phase values correspond to the unsaturated clay-rich top layer and the low permeable Mancos clay at the bottom, whereas the high phase values are associated with the sandy-gravel aquifer material. Nevertheless, it is obvious that the NRA was not accurate enough to detect outliers in the datasets solving for the less-

polarizable anomaly located at ~90 m along profile. The enhanced resolution and the lack of artifacts clearly demonstrate the applicability of and the additional benefit provided by the proposed DCA.

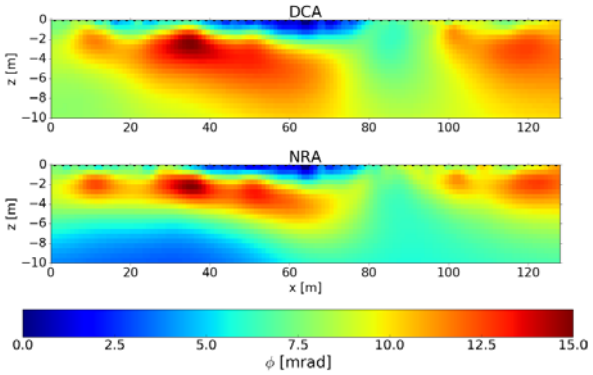

Figure 6. IP imaging results in terms of the phase of the complex electrical resistivity for data processed after the proposed DCA and standard NRA.

After performing the DCA and inversion of the entire dataset, it was possible to construct maps representing the electrical properties of the subsurface at different depths. Figure 7 presents the inverted phase values for aquifer materials (at a depth of 4.5 m), which reveal clear anomalies characterized by high IP values (>10 mrad). Ongoing work consists on the collection of aquifer materials to confirm the presence of NRZ in areas associated to high IP response

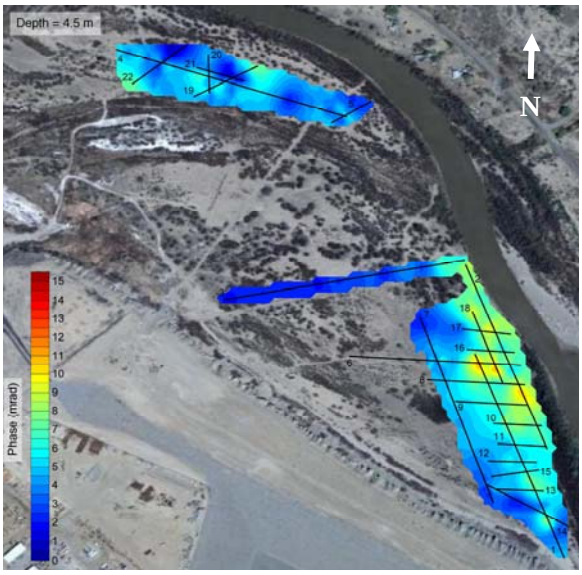

Figure 7. Map of the Shiprock Site presenting the distribution of phase values in aquifer materials (at a depth of 4.5 m).

CONCLUSIONS

We propose a new methodology for the processing of TDIP imaging data sets based on the analysis of the IP decay curve. Our approach reliably identifies outliers and provides an adequate quantification of the data error. Error parameters obtained with the proposed DCA and standard NRA are consistent, which clearly demonstrates the applicability of our approach. Imaging results obtained with the DCA resulted in images with enhanced contrasts and less artefacts compared to those images obtained with the NRA. Based on our results, the new approach is able to improve the quality of IP images.

REFERENCES

Atekwana, E.A., and Slater, L.D., 2009, Biogeophysics: A new frontier in Earth science research: Reviews of Geophysics 47, RG4004.

Dahlin, T., Zhou, B.,. 2006, Multiple-gradient array measurements for multichannel 2D resistivity imaging: Near Surface Geophysics 4(2), 113-123.

Doetsch, J., Ingeman-Nielsen, T., Christiansen, A. V., Fiandaca, G., Auken, E., and Elberling, B., 2015, Direct current (DC) resistivity and induced polarization (IP) monitoring of active layer dynamics at high temporal resolution: Cold Regions Science and Technology, 119, 16-28.

Flores Orozco, A., Kemna, A., Zimmermann, E.,. 2012, Data error quantification in spectral induced polarization imaging: Geophysics 77(3), E227-E237.

Flores Orozco, A., Williams, K.H., Long, P.E., Hubbard, S. S., Kemna, A.,. 2011, Using complex resistivity imaging to infer biogeochemical processes associated with bioremediation of an uranium-contaminated aquifer: Journal of Geophysical Research: Biogeosciences 116(G3), 2156-2206.

Flores Orozco, A., Williams, K.H., Kemna, A.,. 2013, Time-lapse spectral induced polarization imaging of stimulated uranium bioremediation: Near Surface Geophysics: 11(5), 531-544.

Gazoty, A., Fiandaca, G., Pedersen, J., Auken, E., & Christiansen, A. V., 2013, Data repeatability and acquisition techniques for time-domain spectral induced polarization: Near Surface Geophysics, 11(4), 391-406.

Kemna, A., 2000. Tomographic Inversion of Complex Resistivity: Theory and Application, Der Andere Verlag, Osnabrück.

Ntarlagiannis, D., Yee, N., and Slater, L., 2005, On the low-frequency electrical polarization of bacterial cells in sands: Geophysical Research Letters 32, L24402.

Slater, L., Ntarlagiannis, D., Personna, Y.R., and Hubbard, S., 2007, Pore-scale spectral induced polarization signatures associated with FeS biomineral transformations: Geophysical Research Letters 34.

Wainwright, H. M., Flores Orozco, A.., Bücker, M., Dafflon, B., Chen, J., Hubbard, S. S., and Williams, K. H., 2015, Hierarchical Bayesian method for mapping biogeochemical hot spots using induced polarization imaging. Water Resources Research 52, 533-551.

Williams, K.H., Kemna, A., Wilkins, M.J., Druhan, J., Arntzen, E., N'Guessan, A.L., Long, P.E., Hubbard, S.S., and Banfield, J.F., 2009, Geophysical monitoring of coupled microbial and geochemical processes during stimulated subsurface bioremediation: Environmental Science and Technology 43, 6717-6723.